Journal of Zhejiang University-SCIENCE A (Applied Physics & Engineering)
ISSN 1673-565X (Print); ISSN 1862-1775 (Online)
www.zju.edu.cn/jzus; www.springerlink.com
E-mail: jzus@zju.edu.cn

Containment of high-speed rotating disk fragments*

Hai-jun XUAN†, Lu-lu LIU, Yi-ming FENG†, Qing HE, Juan-juan LI

(*High-Speed Rotating Machinery Laboratory, Institute of Chemical Machinery, Faculty of Engineering, Zhejiang University, Hangzhou 310027, China*)

†E-mail: marine@zju.edu.cn; fymlx163@gmail.com

Received Feb. 22, 2012; Revision accepted July 30, 2012; Crosschecked Aug. 15, 2012

Abstract: Disk burst accidents sometimes happen in aeroengines. To avoid tragic consequences, aeroengine casings must have sufficient containment capability. Experiments and simulations need to be conducted to study the impact, distortion, and perforation caused by disk burst and which may give important clues to potential failure mechanisms. This paper presents some containment tests of high-speed rotating disk fragments, in which the original disks were burst into three equal fragments within a predetermined rotating speed range. The failure modes of the containment casing varied significantly with the thickness of the containment casing. Shearing, tearing, tensile fracture, and large plastic stretching deformation occurred in a thin-walled containment casing, while a thick-walled casing could contain disk fragments and withstand large plastic deformation. Numerical simulations were carried out to study the impact process and failure modes further. Good agreement was found between the results of the simulations and the tests.

Key words: Aeroengine, Disk fragments, Engine casing, Containment capability, Numerical simulation
doi:10.1631/jzus.A1200047 **Document code:** A **CLC number:** V232.3

1 Introduction

In modern aeroengine design, engineers should make sure that high-speed fragments can be arrested and contained by the containment casing when a disk burst accident happens. Otherwise, the disk fragments may break through the casing and strike other system components, such as hydraulic pipelines, electrical and signal cables, oil tanks, and the airframe, which may cause fatal results for the airplane and its passengers. Some special disks, such as turbine disks, work mostly in high temperature gradients and are subjected to high rotational velocity which results in large centrifugal forces. These forces and other factors, may cause degradation and burst failure of the critical disks. Even though disk burst accidents happen infrequently nowadays, they are not completely avoidable. Fig. 1 shows a CF6-80A2 engine high pressure turbine disk burst accident that happened at Los Angeles International Airport in June 2006 (Aviation Safety Network, 2006). In 2010, another serious turbine disk burst accident (Fig. 2) was reported in a Qantas A380 engine (Hradecky, 2010). Therefore, it is significant and necessary to study the containment capability of cylindrical casings impacted by disk burst fragments.

Many studies have been devoted to research on engine containment, but mostly on blade containment by metallic casings (Sarkar and Atluri, 1996; Xuan and Wu, 2006; Yuriy and Dmitriy, 2006) and fiber reinforced composite casings (Roberts *et al.*, 2002; Sharda *et al.*, 2006; Naik *et al.*, 2009; Stahlecker *et al.*, 2009). Carney *et al*. (2009) presented a new configuration of a containment casing consisting of a flat plate with a radial convex curve section at the impact point. Their study indicated that the curved surface could force the blade to deform plastically, dissipating

* Project supported by the Chinese Aviation Propulsion Technology Development Program (No. APTD-11), and the Zhejiang Provincial Natural Science Foundation of China (No. Y1090245)

Fig. 1 A CF6-80A2 high pressure turbine disk burst accident which occurred at Los Angeles International Airport (Aviation Safety Network, 2006)

Fig. 2 A Rolls Royce Trent 972 intermediate pressure turbine disk burst accident which occurred near Singapore (Hradecky, 2010)

energy before the full impact of the blade was received by the plate. The curved casing was able to tolerate a higher impact velocity before failure. However, there have been few investigations into disk fragment containment. Teng and Wierzbicki (2008) conducted impact tests on an aircraft engine containment panel obliquely struck by a titanium turbine fragment. Using numerical simulations of impact tests, they also made a comparison between two leading commercial finite element codes, ABAQUS/Explicit and LS-DYNA. A large difference in the calculated energy dissipation was observed. Hagg and Sankey (1974) developed an analytical procedure to predict the containment result of disk burst fragments in a cylindrical shell. They proposed that the containment of missile-like steel disk fragments by a steel cylindrical shell was a sequential two-stage process, and set out the factors of the two stages. However, in view of the limited application of Hagg and Sankey (1974)'s method to other rotating structures due to numerous approximations and simplifications, Stamper and Hale (2008) used ANSYS/LS-DYNA to develop an analysis method that could provide more accurate predictions of containment failure limits for a wide range of disk and containment geometries. The simulation results showed a good correlation with burst data calculated using Hagg and Sankey (1974)'s method, which demonstrated the method's potential as a reliable tool for containment design. Frankenberger (1998) conducted a turbine disk fragment containment test in a UH-1 Huey helicopter. The disk ruptured into three nearly equal sections which were eventually contained within the Kevlar containment casing. According to recent disk burst accidents of aeroengines in service, a disk usually fragments into three roughly equal pieces (Figs. 1 and 2).

As the consequences of failure to contain aeroengine disk burst fragments are severe, studies concerning this issue are important. This paper presents an experiment involving high-speed rotating disk burst fragments impacting on a containment casing, and a corresponding numerical simulation using a nonlinear finite element method, which proved to be a reliable tool and gave results consistent with the test. This paper is divided into four sections. After the Introduction, Section 2 describes the testing facility, procedures and results, while Section 3 addresses the material model and simulation results of all tests, and is followed by the conclusions.

2 Disk fragment containment test

2.1 Test arrangement

Disk fragment containment test was conducted in the high-speed rotor spin testing facility at the High-Speed Rotating Machinery Laboratory (Hi-RoMa Lab.) of Zhejiang University, China. For such tests, ideally, the materials for the disk and containment casing and the working temperature should be the same as those used in an aeroengine. However, in consideration of the testing cost and material accessibility, Chinese standard 45 steel at room temperature was used in the experiment both for the disk and casing, in place of the usual material.

Before tests, material properties were measured on uniaxial tension test specimens of the disk and casing (Table 1). In the tests, a disk of uniform thickness (h) 30 mm, with inner diameter (D_i) 40 mm and outer diameter (D_o) 280 mm, was fixed on the top end of a high-speed vertical rotating shaft. The containment casing was circular and unflanged, supported by three symmetrically located legs (Fig. 3). Three tests were designed for the investigation by means of fabricating three containment casings with the same inner diameter (D_{ci}) but different wall thickness (δ). The three tests were designed as uncontained, close to critical contained, and contained, respectively. Dimensional parameters of the disk and the containment casing are presented in Table 2.

According to the accident records of engine rotor disk ruptures in service, a rotating disk generally breaks into three fragments of roughly uniform size and shape due to centrifugal force, so the disks were pre-notched with three symmetrical radial through-thickness cracks from the outside to the inside. The notches with a pre-notched length (l) caused a stress concentration which was sufficient to induce the rotating disk to rupture at the desired speed. Enamel covered circuit wire of 0.3 mm diameter was affixed to the inner wall surface of the casing and connected to the signal line of the tester automatic control system to make up the special triggering system. When the disk burst fragments impact on the casing, the circuit is cut off triggering the control system, then the motor auto-stops quickly with the flexible shaft.

2.2 Test results

Experimental data of the disk burst speed (n_{off}) and kinetic energy of a 1/3rd disk fragment (E_K) in the three tests are listed in Table 3. Post-test rearranged fragments of the disk and the containment casing for the three tests are presented in Fig. 4. Among the three test results, small differences in the final pre-notched length l could account for the variance of the disk burst speed.

In test 1 (Fig. 4a), the disk fragments were not contained when the disk burst at a speed of 11 605 r/min. Three relatively uniform sized pieces of the containment casing separated at three symmetrical locations with an angular interval of 120°, which revealed that the three disk fragments burst out almost

Table 1 Material properties of the disk and the containment casing measured in uniaxial tension

Material property	Value	
	Disk	Casing
Yield stress, σ_s (MPa)	650	645
Ultimate stress, σ_b (MPa)	837	841
Stress at fracture, σ_f (MPa)	687	678
Elastic modulus, E (GPa)	203	202
Elongation, δ (%)	17.7	19.0
Reduction of area, ψ (%)	48.5	47.9

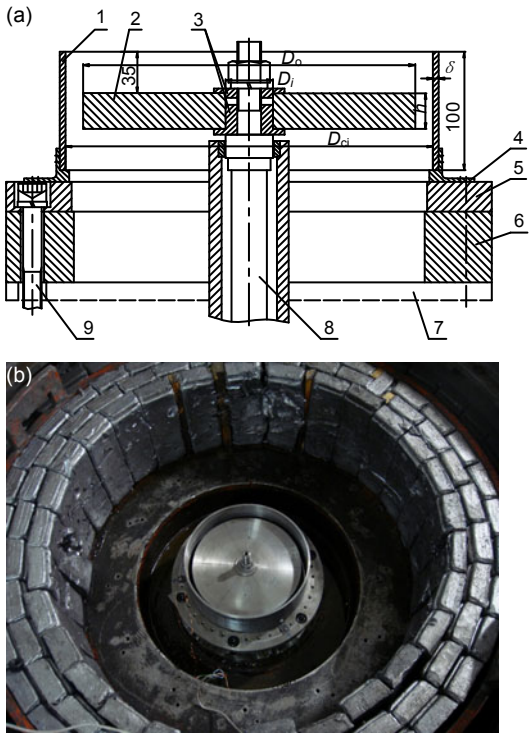

Fig. 3 Test rig sketch (a) and pretest photo in testing chamber (b)
The unit is mm. 1: containment casing; 2: disk; 3: fixture; 4: casing supporting leg; 5: supporting ring; 6: supporting blocks; 7: testing chamber floor; 8: flexible shaft; 9: fixed bolts

Table 2 Dimensional parameters of the disk and the containment casing

No.	Containment casing		Disk			
	δ (mm)	D_{ci} (mm)	D_i (mm)	D_o (mm)	h (mm)	l^* (mm)
1	4					107.1
2	6	304	40	280	30	107.6
3	8					107.5

* l is the final value of the notch length

simultaneously. There were continuous impacts, and three sliding dents along the disk rotating direction at intermediate height were left on the inner wall surface of the containment casing. The same phenomenon was observed in the other two tests. The failure pattern of the containment casing was shearing and tensile fracture with large plastic deformation. The kinetic energy of the disk fragments was dissipated by shearing, extensive bending, and stretching deformation of the casing, plus sliding friction between the casing and the disk fragments. Compared with the other two tests, the thinner containment casing impacted with about the same kinetic energy, but suffered more bending and stretching deformation and tore into three pieces (Fig. 4).

Table 3 Experimental data of the three tests

No.	n_{off} (r/m)	E_K (J)	Containment result
1	11 605	34 743	Uncontained
2	11 523	34 253	Uncontained
3	11 531	34 301	Contained

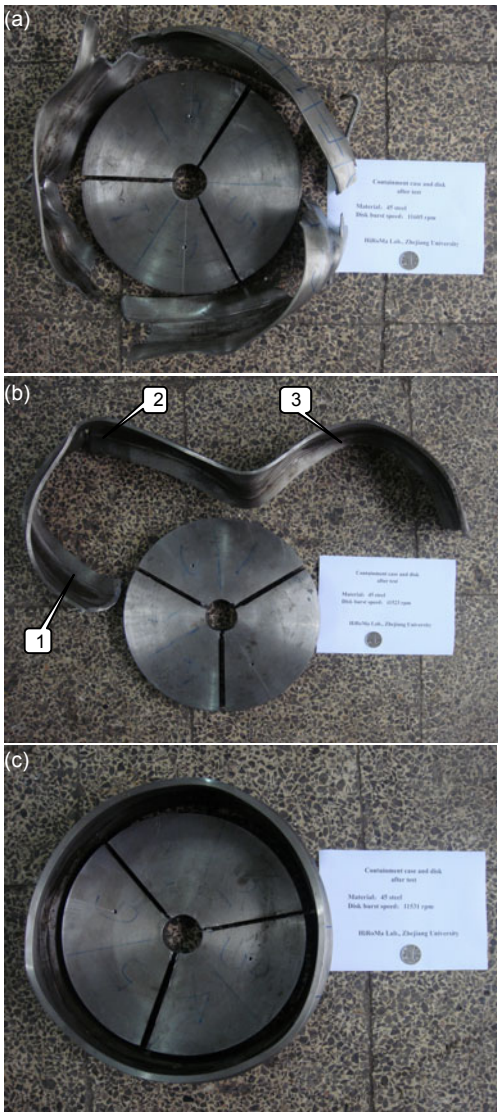

Fig. 4 Post-test rearranged fragments of disk and containment casing for test 1 (a), test 2 (b) and test 3 (c)

Test 2 was designed to be a critical containment casing. The post-test scene in Fig. 4b shows that the containment casing was torn apart at the position marked '1' but the disk fragments did not have enough energy to tear the casing into three parts at the positions marked '2' and '3'. The containment casing was not perforated upon the initial impact. Afterwards, the disk fragments slid ahead along the inner wall of the casing in the rotating direction. But under the shear force produced by the outside edges of the disk fragments, three crack bands were created on the wall of the casing with the width almost equal to the thickness of the disk. At the same time, a short crack not long enough to generate a slit also formed in the impact zone marked '2'. The containment casing after the test had a large amount of deformation, while the disk fragments were nearly undeformed, as in the other two tests. In addition, a concave impact region could be seen in the zone marked '3'. From these test results, it can be concluded that the dissipation of the kinetic energy is due to shear deformation and sliding friction in the impact region followed by extensive bending and stretching deformation due to structural excitation, as also found by Gerstle (1975). The failure pattern of the containment casing is plastic stretching deformation, shearing and tensile fracture. This is consistent with test 2 being close to critical containment.

In test 3 (Fig. 4c), all the disk fragments were successfully contained within the cylindrical casing. Under the impact of the three roughly equal fragments, the containment casing deformed from a circular to an oval-triangle shape. It can be inferred that the disk fragments impacted with each other and slid along the inside wall surface of the casing for a long time, until the kinetic energy of the disk fragments had completely dissipated. The dissipation of the disk fragments' kinetic energy was due mainly to extensive bending, stretching deformation and sliding friction in the impact region of the cylindrical casing.

All the tests were conducted according to the predesigned purpose. It is clear that the containment capability of the casing improved with the increasing thickness of the wall.

3 Numerical simulation and analysis

It is difficult to obtain more useful information during the testing process, but numerical simulation may offer more information. So the three tests were all simulated, and the results were compared with those derived from the tests in order to validate the numerical model. Some test results discussed in Section 2.2 were also used to develop the material model.

3.1 Material model

For the ductile materials of the disks and casings, the Johnson-Cook (J-C) model was employed. The J-C model takes into account high strain rate sensitivity, large deformation, and material softening due to adiabatic heating and damage, so it is quite well suited to problems of metal impact and penetration. Johnson and Cook (1983) expressed the von Mises flow stress as

$$\sigma_y = \left[A + B(\bar{\varepsilon}^{\mathrm{p}})^n\right]\left[1 + C\ln\left(\frac{\dot{\bar{\varepsilon}}^{\mathrm{p}}}{\dot{\varepsilon}_0}\right)\right]\left[1 - T^{*m}\right], \quad (1)$$

where A is the yield stress, B is a material constant, n is the hardening parameter, C is the strain rate sensitivity, m is the temperature sensitivity parameter, $\bar{\varepsilon}^{\mathrm{p}}$ is the effective plastic strain, $\dot{\bar{\varepsilon}}^{\mathrm{p}}$ is the effective plastic strain rate, $\dot{\varepsilon}_0$ is a reference strain rate, and T^* is the non-dimensional temperature defined as follows:

$$T^* = (T - T_0)/(T_{\mathrm{melt}} - T_0), \quad T_0 \le T \le T_{\mathrm{melt}}, \quad (2)$$

where T is the current temperature, T_{melt} is the melting point temperature, and T_0 is the room temperature. The expression in the first set of brackets gives the stress as a function of strain for $\dot{\bar{\varepsilon}}^{\mathrm{p}} / \dot{\varepsilon}_0 = 1.0$ and $T^* = 0$. The expressions in the second and third sets of brackets represent the effects of strain rate and temperature, respectively.

The fracture model proposed by Johnson and Cook (1985) includes a damage parameter D, which is summed over all increments of deformation, and defined as

$$D = \sum \frac{\Delta\varepsilon_{\mathrm{p}}}{\varepsilon_{\mathrm{f}}}, \quad (3)$$

where $\Delta\varepsilon_{\mathrm{p}}$ is an increment of accumulated equivalent plastic strain that occurs during an integration cycle, and ε_{f} is the equivalent strain at fracture. ε_{f}, is assumed to be dependent on a non-dimensional plastic strain rate, $\dot{\varepsilon}^* = \dot{\bar{\varepsilon}}^{\mathrm{p}}/\dot{\varepsilon}_0$, a dimension-less pressure-deviatoric stress ratio ($\sigma^* = p/\sigma_{\mathrm{eff}} = -R_\sigma$, where p is the pressure and σ_{eff} is the effective stress) and a non-dimensional temperature T^*. Under the conditions of strain rate, temperature, pressure and equivalent stress, fracture is then allowed to occur when D=1.0. The general expression for the strain at failure ε_{f} is

$$\varepsilon_{\mathrm{f}} = \left[D_1 + D_2\exp(D_3\sigma^*)\right]\left[1 + D_4\ln\dot{\varepsilon}^*\right]\left[1 + D_5T^*\right], \quad (4)$$

where D_1, D_2, …, D_5 are failure constants determined from material tests. When this failure criterion is met, the deviatoric components of stress are set to zero and remain zero during the rest of the analysis. The element kill algorithm is used to delete the failed elements from the mesh.

3.2 Numerical model and simulation results

In the three simulations, the geometric configurations of the disk and containment casing were the same as those used in the tests. The finite element model (Fig. 5) consisted of a containment casing with a support underneath, and three initially separated and symmetric disk fragments, each with an angular velocity corresponding to the burst speed in the test. In the model, crack propagation was simplified by assuming that the crack time was zero, causing three equal disk fragments to separate from each other at the start of calculations. For each containment casing, the element density was uniform with an element size of 0.995 mm in the circumferential direction, 1.0 mm in the height direction, and 1.0 mm in the through-thickness direction. There was no need to mesh the disk fragments with smaller element sizes because

their deformation was very small according to the test results. By default, the element type employs one point integration plus viscous hourglass control for faster element formulation. This is advantageous in terms of computation time savings and robustness in cases of large deformation. Single surface contact was chosen as the contact type, and the effect of friction between the disk fragments and the containment casing was also taken into account. The material parameters of the 45 steel used in the simulation are listed in Table 4 and are taken from Chen *et al.* (2007).

Figs. 6–8 show the simulation results at different times for the three tests, respectively. The total time of each simulation was 3.0 ms. For the simulation of test 1, von Mises stress contour plots at four different time points are shown in Fig. 6. The failure patterns of the containment casing are shearing, tensile fracture

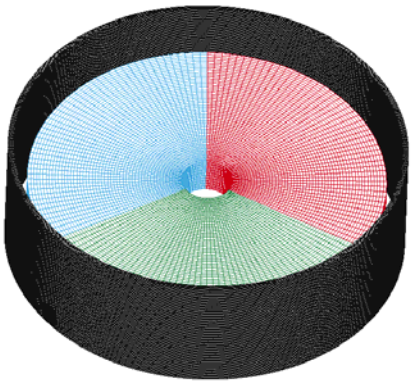

Fig. 5 Initial finite element model

Table 4 Parameters of 45 steel used to define the Johnson-Cook (J-C) material and fracture model

Parameter	Value	Parameter	Value	Parameter	Value
J-C constitutive relation constant		J-C fracture criterion constant		Physical constant	
$\dot{\varepsilon}_0$ (s^{-1})	1	D_1	0.10	E (GPa)	200
A (MPa)	630	D_2	0.76	v	0.3
B (MPa)	822	D_3	1.57	P (kg/m^3)	7.8×10^3
C	0.064	D_4	0.005	T_m (K)	1795
n	0.47	D_5	−0.84	T_r (K)	300
m	1.06				

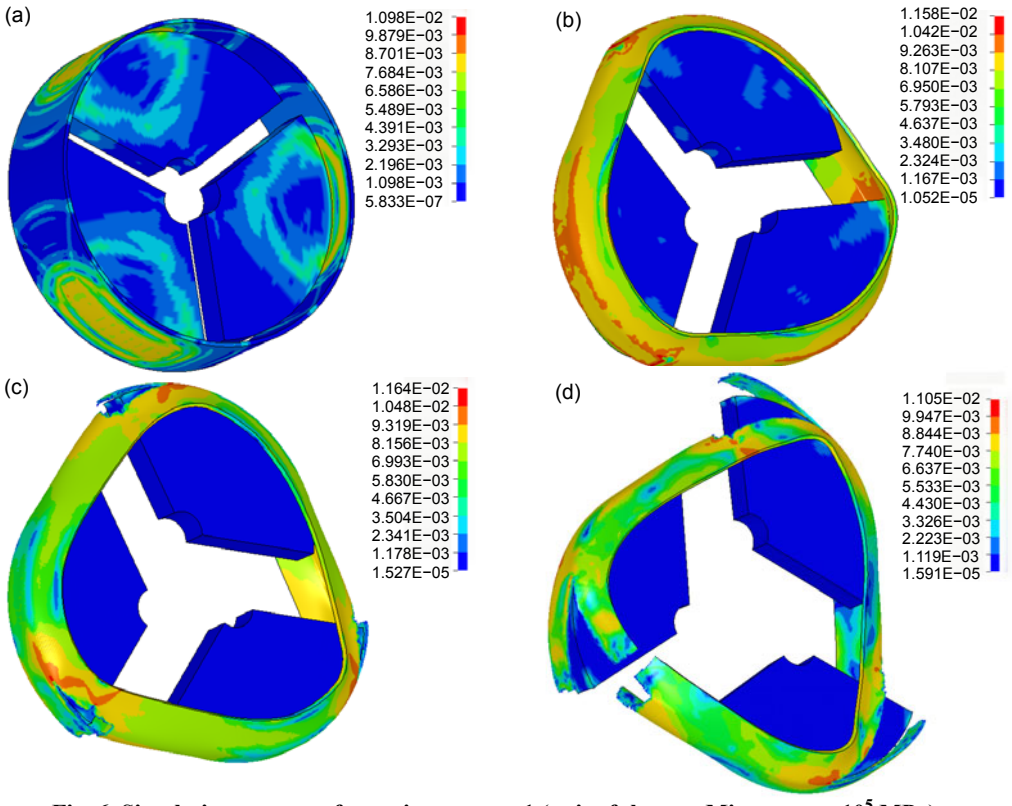

Fig. 6 Simulation process of containment test 1 (unit of the von-Mises stress: 10^5 MPa)
(a) t=0.48 ms; (b) t=0.93 ms; (c) t=1.26 ms; (d) t=1.86 ms

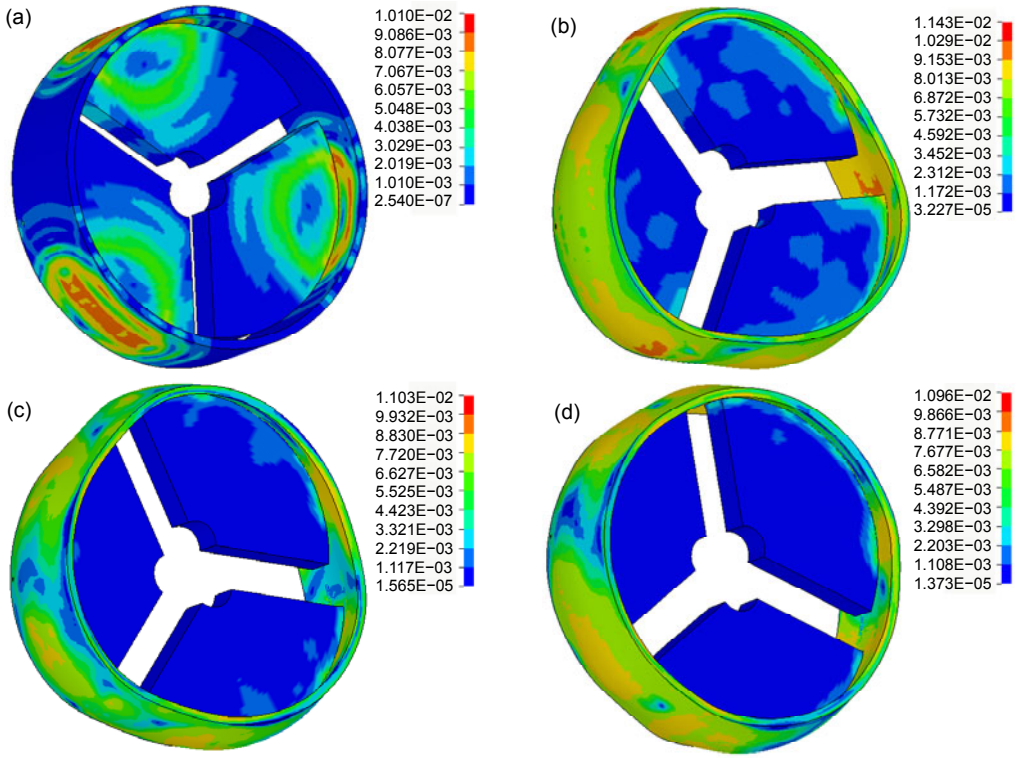

Fig. 7 Simulation process of containment test 3 (unit of the von-Mises stress: 10^5 MPa)
(a) t=0.48 ms; (b) t=0.90 ms; (c) t=1.29 ms; (d) t=1.89 ms

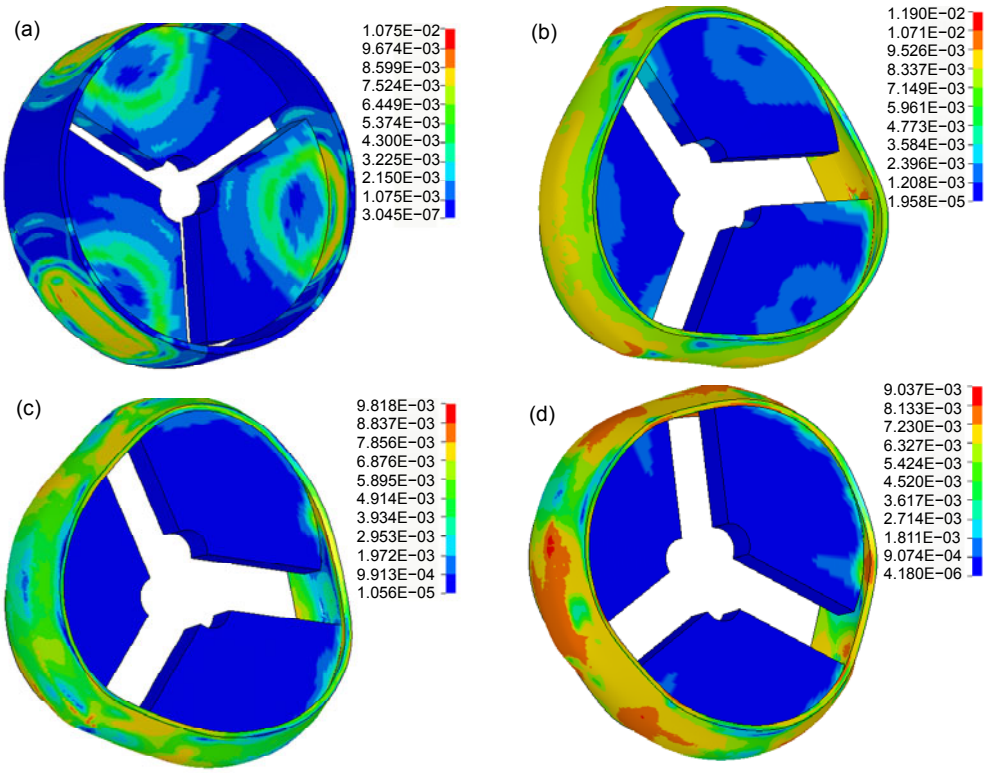

Fig. 8 Simulation process of containment test 2 (unit of the von-Mises stress: 10^5 MPa)
(a) t=0.48 ms; (b) t=0.96 ms; (c) t=1.32 ms; (d) t=2.10 ms

and large plastic deformation, which closely match the failure patterns found in the test (Fig. 4a). Large plastic deformations occur in the casing and continue until 0.93 ms, then tension cracks occur on the outer surface of the casing. As the disk fragments continue to impact the casing, the cracks propagate quickly and then the casing breaks into pieces at 1.86 ms. Surprisingly, we found that asymmetries occurred in the result because the finite element model included element failure. These were also observed by Stamper and Hale (2008). They pointed out that the inclusion of element failure and subsequent erosion led to asymmetric results despite the use of symmetry in mesh, boundary conditions and impact loads. In the simulation of test 1, the disk fragments fly out after the containment casing is torn up. After the disk fragments impact on the containment casing, the kinetic energy decreases and the plastic deformation energy increases for both the disk fragments and the containment casing. However, the energy absorbed by plastic deformation of the disk fragments is small, which is consistent with the facts observed in the tests that the disk fragments remained almost undeformed and that upon the initial impact the energy dissipated fast through the containment casing by plastic deformation, but then dissipated more slowly.

For the simulation of test 3, von Mises stress contour plots at four different time points are shown in Fig. 7. Some elements eroded on the inner wall surface of the casing under the impact of the disk fragments. Global plastic deformation occurs on the casing which finally takes on an oval-triangle shape, while the disk fragments are almost undeformed, which is in agreement with the test result shown in Fig. 4c. The 8 mm-thick casing wall begins to be impacted by the three disk fragments at 0.48 ms and subsequently generates plastic bending and stretching deformation till the end of the simulation. Due to the frictional interaction between the casing and the disk fragments, the containment casing finally rotates together with the disk fragments.

For the simulation of test 2, von Mises stress contour plots at four different time points are shown in Fig. 8, The results show that the casing contains the disk fragments, contrary to the experimental result shown in Fig. 4b. Many factors may have contributed to the differences between the simulation and the test. Firstly, test 2 was designed close to the critical containment. It is well known that consistency is very difficult to obtain between simulations and tests near the critical point, where the final results are very sensitive to small changes in initial conditions such as the ballistic limit in the armor piercing field. Secondly, the descriptions of the dynamic behaviors of the material can be violated if improper material models or model-related parameters are used. It is still a huge challenge for researchers to describe accurately the dynamic behaviors of materials. Last but not least, some other factors, such as the mesh size, the boundary conditions and the contact-impact descriptions, also have large effects on consistency.

Comparisons of the tests and relative simulation results can be made from Fig. 4 and Figs. 6–8. The nonlinear simulation method used in this study could be a reliable way to analyze an aeroengine containment capability in similar disk burst cases.

4 Conclusions

Tests of disk burst fragments impacting on containment casings and corresponding numerical simulations using a nonlinear finite element method are presented in this paper. Based on this investigation, some conclusions can be drawn as follows:

1. For identical disk fragments with nearly the same burst speed, failure patterns vary significantly depending on the thickness of the containment casing wall. Shearing, tearing and tensile fracture plus extensive stretching deformations occur for thinner containment casings; however, large plastic bending, stretching deformation and friction are the main energy absorption modes for thicker containment casings which could contain the disk burst fragments.

2. This study demonstrates that the nonlinear finite element method used in this paper is an alternative and reliable tool for aeroengine containment structure design.

References

Aviation Safety Network, 2006. Aircraft Accident Boeing 767-223 ER N330AA Los Angeles International Airport. Available from: http://aviation-safety.net/database/record.php?id=20060602-0 [Accessed on Feb. 17, 2008]

Carney, K.S., Pereira, J.M., Revilock, D.M., Matheny, P., 2009. Jet engine fan blade containment using an alternate geometry. *International Journal of Impact Engineering*, **36**(5):720-728. [doi:10.1016/j.ijimpeng.2008.10.002]

Chen, G., Chen, X., Chen, Z.F., Qu, M., 2007. Simulation of A3 steel blunt projectile impacting 45 steel plates. *Explosion and Shock Waves*, **27**(5):390-397 (in Chinese).

Frankenberger, C.E., 1998. FAA T53-L-13L Turbine Fragment Containment Test. Report No. DOT/FAA/AR-98/22, Federal Aviation Administration, Washington.

Gerstle, J.H., 1975. Analysis of rotor fragment impact on ballistic fabric engine burst containment shields. *Journal of Aircraft*, **12**(4):388-393. [doi:10.2514/3.44461]

Hagg, A.C., Sankey, G.O., 1974. The containment of disk burst fragments by cylindrical shells. *Journal of Engineering for Power*, *Transaction of the ASME*, **96**:114-123. [doi:10.1115/1.3445758]

Hradecky, S., 2010. Accident: Qantas A388 near Singapore on Nov 4th 2010, Uncontained Engine Failure. The Aviation Herald. Available from: http://avherald.com/h?article=43309c6d&opt=0 [Accessed on Feb. 11, 2012]

Johnson, G.R., Cook, W.H., 1983. A Constitutive Model and Data for Metals Subjected to Large Strains, High Strain Rates and High Temperatures. Proceedings of the Seventh International Symposium on Ballistics, Hague, the Netherlands. [doi:10.1038/nrm3209]

Johnson, G.R., Cook, W.H., 1985. Fracture characteristics of three metals subjected to various strains, strain rates, temperatures and pressures. *Engineering Fracture Mechanics*, **21**(1):31-48. [doi:10.1016/0013-7944(85)90052-9]

Naik, D., Sankaran, S., Mobasher, B., Rajan, S.D., Pereira, J.M., 2009. Development of reliable modeling methodologies for fan blade out containment analysis-Part I: Experimental studies. *International Journal of Impact Engineering*, **36**(1):1-11. [doi:10.1016/j.ijimpeng.2008.03.007]

Roberts, G.D., Revilock, D.M., Binienda, W.K., Nie, W.Z., Mackenzie, S.B., Todd, K.B., 2002. Impact testing and analysis of composites for aircraft engine fan cases. *Journal of Aerospace Engineering*, **15**(3):104-110. [doi:10.1061/(ASCE)0893-1321(2002)15:3(104)]

Sarkar, S., Atluri, S.N., 1996. Effects of multiple blade interaction on the containment of blade fragments during a rotor failure. *Finite Elements in Analysis and Design*, **23**(2-4):211-223. [doi:10.1016/S0168-874X(96)80008-4]

Sharda, J., Deenadayalu, C., Mobasher, B., Rajan, S.D., 2006. Modeling of multilayer composite fabrics for gas turbine engine containment systems. *Journal of Aerospace Engineering*, **19**(1):38-45. [doi:10.1061/(ASCE)0893-1321(2006)19:1(38)]

Stahlecker, Z., Mobasher, B., Rajan, S.D., Pereira, J.M., 2009. Development of reliable modeling methodologies for engine fan blade out containment analysis. Part II: Finite element analysis. *International Journal of Impact Engineering*, **36**(3):447-459. [doi:10.1016/j.ijimpeng.2008.08.004]

Stamper, E., Hale, S., 2008. The Use of LS-DYNA Model to Predict Containment of Disk Burst Fragments. 10th International LS-DYNA Users Conference, Dearborn, Michigan.

Teng, X., Wierzbicki, T., 2008. Gouging and fracture of engine containment structure under fragment impact. *Journal of Aerospace Engineering*, **21**(3):174-186. [doi:10.1061/(ASCE)0893-1321(2008)21:3(174)]

Xuan, H.J., Wu, R.R., 2006. Aeroengine turbine blade containment tests using high-speed rotor spin testing facility. *Aerospace Science and Technology*, **10**(6):501-508. [doi:10.1016/j.ast.2006.04.006]

Yuriy, N.S., Dmitriy, V.G., 2006. Numerical Analysis of Aircraft Engine Fan Blade-Out. 42nd AIAA/ASME/SAE/ASEE Joint Propulsion Conference & Exhibit, Sacramento, California.